Nanotechnology in Biomaterials

JOURNAL OF
biomaterials
applications

Journal of Biomaterials Applications
2022, Vol. 36(6) 996–1010

DOI: 10.1177/08853282211045770
journals.sagepub.com/home/jba
SAGE

Further structural characterization of ovine forestomach matrix and multi-layered extracellular matrix composites for soft tissue repair

Matthew J Smith[1], Sandi G Dempsey[1], Robert WF Veale[1], Claudia G Duston-Fursman[1], Chloe A F Rayner[1], Chettha Javanapong[1], Dane Gerneke[2], Shane G Dowling[1], Brandon A Bosque[1], Tanvi Karnik[1], Michael J Jerram[1], Arun Nagarajan[1], Ravinder Rajam[1], Alister Jowsey[1], Samuel Cutajar[1], Isaac Mason[1], Roderick G Stanley[1], Andrew Campbell[1], Jenny Malmstrom[3], Chris H Miller[1] and Barnaby C H May[1]

Abstract

Decellularized extracellular matrix (dECM)–based biomaterials are of great clinical utility in soft tissue repair applications due to their regenerative properties. Multi-layered dECM devices have been developed for clinical indications where additional thickness and biomechanical performance are required. However, traditional approaches to the fabrication of multi-layered dECM devices introduce additional laminating materials or chemical modifications of the dECM that may impair the biological functionality of the material. Using an established dECM biomaterial, ovine forestomach matrix, a novel method for the fabrication of multi-layered dECM constructs has been developed, where layers are bonded via a physical interlocking process without the need for additional bonding materials or detrimental chemical modification of the dECM. The versatility of the interlocking process has been demonstrated by incorporating a layer of hyaluronic acid to create a composite material with additional biological functionality. Interlocked composite devices including hyaluronic acid showed improved *in vitro* bioactivity and moisture retention properties.

Keywords

hyaluronic acid, decellularized extracellular matrix, ovine forestomach matrix, angioconduction, keratinocyte, cell migration, wound healing

Introduction

Decellularized extracellular matrix (dECM) bioscaffolds are now used in all aspects of modern soft tissue repair and regeneration, including the treatment of acute and chronic wounds, plastic and reconstructive surgery and implant procedures to reinforce and repair missing or damaged soft tissue. dECM bioscaffolds are mimics of soft tissue extracellular matrix (ECM), retaining both the structure and composition of tissue ECM.[1,2] Allogenic and xenogeneic dECM bioscaffolds from various source tissues have been shown to provide a structural and biochemical framework that supports cell growth, differentiation and proliferation, with the scaffold being ultimately remodelled into regenerated soft tissue.[3,4]

Ovine forestomach matrix (OFM) is a dECM bioscaffold prepared from decellularized propria submucosa isolated from ovine forestomach tissue.[5] Ovine forestomach matrix retains the native collagen structure seen in normal tissue ECM,[6] as well as functional secondary molecules required for cell adhesion, migration, proliferation and rapid development of capillary networks.[5,7–9] OFM has been used as

[1]Department of Research and Clinical Development, Aroa Biosurgery Limited, Auckland, New Zealand
[2]Auckland Bioengineering Institute, The University of Auckland, Auckland, New Zealand
[3]Department of Chemical and Materials Engineering, The University of Auckland, Auckland, New Zealand

Corresponding author:
Barnaby C H May, Department of Research and Clinical Development, Aroa Biosurgery Limited, 2 Kingsford Smith Place, Mangere, Auckland 2022, New Zealand.
Email: barnaby.may@aroabio.com

a universal building block for the design of devices for soft tissue repair, either as single layers of dECM (~200 μm thick), powders or multi-layered devices (up to ~3 mm thick) [10,11]; and as a platform for further functionalization such as antimicrobial dECM devices.[12] OFM-based devices have been adopted into regular clinical practice for the treatment of acute and chronic wounds,[13–17] reconstructive surgery[18–21] and abdominal wall repair.[22,23] Xenograft-derived dECM for human soft tissue repair have been utilized for decades. One of the most common xenograft source material is derived from porcine tissues. Severe inflammatory reactions to porcine tissue are well documented[24,25] and further, there are strict cultural and religious laws that ban the use of porcine products, even for medical purpose.[26] To date, there have been no documented severe inflammatory reactions to ovine tissue and no cultural or religious exclusions of note. Further, the rumen of ovines is high vascularized, facilitates high cell turnover and is a physically large organ to sustainably maximize the use of this source tissue.[27]

In order to further expand the potential applications of dECM bioscaffolds across the variety of soft tissue repair procedures; multi-layered devices have been developed whereby individual layers of dECM are physically laminated to create thicker designs. A range of techniques have been explored to laminate layers of dECM, including dehydrothermal lamination via vacuum drying,[28] lyophilization,[10] chemical cross-linking[29–31] adhesives[32] and suture embroidery.[10] The primary aim of these multi-layered designs is to increase the device biomechanical strength and physical properties to meet specific clinical indications. Further, multi-layered dECM devices would better facilitate healing by providing more useful layers for the integration of migrating host cells for host response as well as a greater number of bio-available key secondary proteins and growth factors. For example, the design of reinforced OFM devices incorporating embroidery to sew single layers of OFM into thicker multi-layered constructs using suture filament (e.g. polyglycolic acid, PGA) has been previously reported.[10] These thicker OFM-based biomaterials have improved uniaxial and biaxial strength, enabling optimization of device biomechanical properties toward specific clinical applications where single layer dECM material would not be suitable, for example, hernioplasty .[10]

Driving principles in the development of dECM bioscaffolds are to limit or reduce any potential adverse inflammatory response to the material, retain important secondary molecules that aid tissue regeneration, and ensure the delicate native structure of the tissue ECM is not damaged.[33,34] As such, processing of these materials is highly optimized to remove potentially inflammatory cell components while maintaining the structure and important bioactive secondary molecules present in tissue ECM. Current methods of creating multi-layered dECM devices often come at the expense of the biological properties. For example, chemical crosslinking is effective in laminating sheets of dECM. However, the inclusion of covalent modifications to the dECM reduces the biomechanical performance of the resultant laminate,[10,35] as well as negatively impacting the inflammatory response.[29,36] During normal wound healing, circulating and resident macrophage cells respond to tissue damage based on spatial cues in a tightly controlled, time dependent manner.[37] In acute wound healing, macrophage cells provide an initial pro-inflammatory response, followed by a pro-wound healing and finally a pro resolving response. Multiple *in vivo* studies have demonstrated that cross-linked dECM scaffolds can lead to a prolonged inflammatory response compared with non-crosslinked materials; this may be due to the chemical and structural modifications to native ECM proteins inducing a foreign body response, preventing the normal transition from inflammatory response to the wound healing and resolution responses in macrophages and other inflammatory cells.[38,39]

The present study reports a novel physical method of creating multi-layered dECM devices, without the need for introducing additional components, modifying ECM biochemistry or denaturation of the ECM structure. Cross-linking of OFM was ruled out due to the well characterized negative inflammatory response evoked by cross-linking collagen-based biomaterials.[40–42] In this way, dECM structural and biological properties remain preserved to promote cellular infiltration, proliferation and constructive remodelling. The process described herein utilized a method of physically interlocking OFM sheets, such that the resultant devices retained the open porous dECM architecture, native collagen organization, and tissue structures such as residual vascular channels. Furthermore, the versatility of the fabrication method also enabled the creation of composite devices, exhibited through the incorporation of hyaluronic acid (HA) to provide additional biological functionality without damaging modification to the dECM structure, whilst retaining the biological properties of HA. Hyaluronic acid is a natural and linear polysaccharide, consisting of repetitive disaccharide units of D-glucuronic acid and N-acetyl-D-glucosamine bound by β (1→3) and β (1→4) glycosidic bonds. It is a major component of the ECM and plays an important role in supporting cells during the wound healing process,[43,44] recognition by specific surface receptors during healing process,[45] collagen deposition and angiogenesis.[46] This represents a new technique for the fabrication of multi-layered dECM devices with advantages of being non-damaging to the dECM biological and structural properties and enabling the inclusion of additional biomolecules for tailored functionality and biological response in soft tissue repair.

Materials and methods

General

Lyophilized OFM material was produced from propria submucosa of the ovine forestomach (rumen) extracted from New Zealand animals <12 months old, according to proprietary methods (Aroa Biosurgery Ltd, Auckland, New Zealand) (Lun, Irvine et al. 2010). Hyaluronic acid sodium salt (MW 1.0 MDa) (Glentham Life Sciences, Wiltshire, United Kingdom) was used to produce a glycosaminoglycan (GAG) foam ('GAGF') via a proprietary process, whereby 1.25% w/v HA was dispersed in reverse osmosis water (ROH_2O) and lyophilized for a total of 21 h. All mechanical testing was conducted using a Shimadzu AGS-X universal testing system (UTS). Unless otherwise stated, all test samples were terminally sterilized using ethylene oxide (EO) (BSN Medical; Auckland, New Zealand). Immortalised keratinocyte cells[47] (HaCaT) were cultured in Dulbeccós modified Eaglés Medium (DMEM) (Gibco; 12,100–046) supplemented with 5% FBS (Gibco; 10,091–148) and 1% L-Glutamine–Penicillin–Streptomycin (Gibco; 10,378–016) in a 5% CO_2 atmosphere with 95% humidity at 37°C. Statistical significance was calculated via t-test using Minitab software (Pennsylvania, United States).

Fabrication

Multi-layered OFM devices were manufactured via a proprietary process using interlocking tabs (Aroa Biosurgery Ltd, Auckland, New Zealand). Briefly, a single sheet of lyophilized OFM was pierced to cut an array of small circular flaps in the material measuring approximately 2.5 mm ± 0.5 mm in diameter, termed 'tabs'. Additional layers of lyophilized OFM were perforated to produce an array of piercings (~0.7 mm diameter) in the material. The tab cut OFM sheet and perforated OFM sheets were aligned and tabs mechanically forced through the piercings, physically interlocking the individual dECM layers together (Figure 1). Tabs and associated perforations were spaced in a grid approximately 3.5 mm apart. Layered devices comprising three (3-layer, 'OFM-3') or five OFM layers (5-layer, 'OFM-5') were prepared according to this method. A composite design ('CMP') was also prepared using the interlocking method by incorporating a single layer of GAGF, to yield a configuration of; OFM-GAGF-OFM-OFM (Figure 1(a)).

Atomic force microscopy

Terminally sterilized samples of OFM samples were imaged using an Asylum Research Cypher ES atomic force microscope (AFM) (Oxford Instruments, Goleta, CA). The samples were epoxied to mild steel pucks, followed by sectioning by hand using a scalpel to expose the matrix interior. The images were acquired in air, using tapping mode with a Tap 300 probe (Budget Sensors, Sofia, Bulgaria). The amplitude was tuned to 1 V and the images were acquired at a setpoint of 570 mV using a scan speed of 1 Hz and a resolution of 512 points and lines. Height, phase and amplitude were recorded, with an amplitude representing the feedback channel. Presented height images have been subjected to an XY planefit using the AR16 plugin in IgorPro and 3D rendering of the images was performed using the same software.

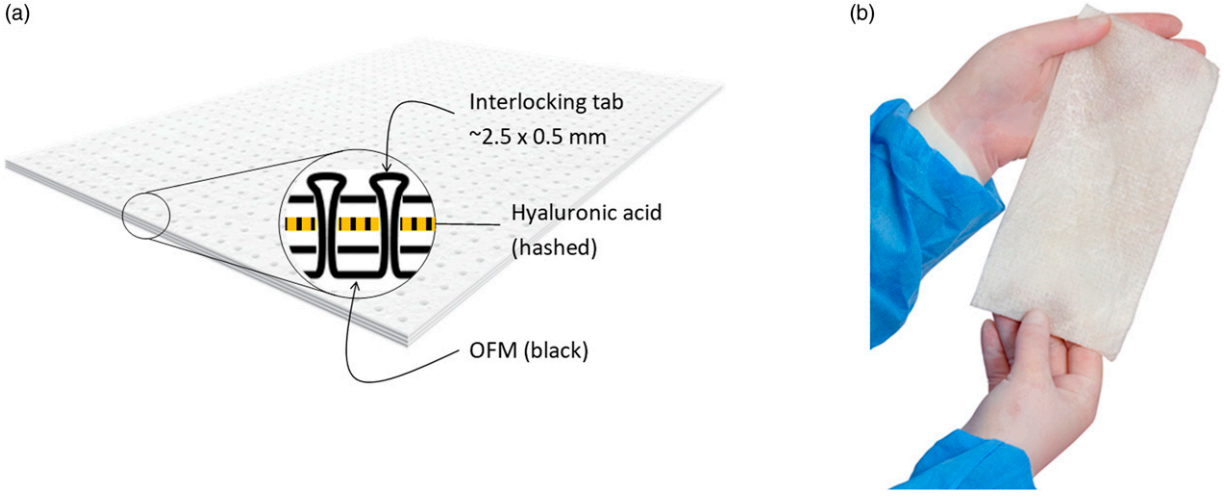

Figure 1. (a). Simplified cross-section schematic of a composite device ('CMP'), comprising OFM (black) and a layer of HA (hashed). Layers are interlocked via a 'tab' penetrating cross-sectionally through the layers. (b). Representative photograph of a hydrated layered device fabricated using the interlocking fabrication process. OFM: Ovine forestomach matrix-3; CMP: composite samples.

Dye perfusion

A solution of crystal violet (Sigma-Aldrich, St Louis, MO) (0.1% w/v) was prepared in ROH_2O, and membrane filtered (0.22 μm), then further diluted 1:3 with glycerol (Thermo Fisher Scientific, Waltham, MA). The working dye solution was injected into the large residual vascular channels from the mucosal side of hydrated OFM using an insulin syringe (Becton Dickinson, Franklin Lakes, NJ). The dye solution was gently and slowly perfused through the vessel then imaged via IR-ADV C5550 scanner (Canon, Tokyo, Japan). Images were adjusted for brightness and contrast using ImageJ software (US National Institutes of Health, Bethesda, MD).

Micro-computed tomography

Representative OFM sub-samples measuring 5 mm x 8 mm were vapour stained for 3 days above a 1% solution of aqueous OsO_4 (Sigma Aldrich). The samples were mounted using 4.5 mm straws for imaging using a SKYSCAN 1272 micro-CT instrument (Bruker, Billerica, MA). Instrument parameters used were as follows; X-ray voltage=54 kV; beam current=200 mA; exposure time=4000 mS; camera pixels=4904 × 3280 pixels; aluminium filter=0.25 μm. Datasets were collected using 0.15° rotation step, 180° rotation, 2 x frame averaging over a 3–5 h period per sample. The micro-CT data were reconstructed to give greyscale transaxial planes using InstaRecon software (InstaRecon, Champaign, IL). DataViewer (Bruker, Billerica, MA) software was then used to align and select a small volume of interest (VOI). CTVox (Bruker, Billerica, MA) software was used to visualize volumes in 3D.

Uniaxial

Test materials were cut using a dog bone die (ASTM D638 Type IV), providing samples with a width of 6 mm and gauge length of 25 mm. The thickness of each sample was measured using a digital thickness gauge (Insize, Spain) and determined as the mean of three measurements along the gauge length. Samples (n = 19) were then fully rehydrated via immersion in room-temperature phosphate-buffered saline (PBS) for 5 min prior to testing. Force (N) was measured using a 100 N load cell and extension was measured from crosshead displacement (25.4 mm/min).

Biaxial (ball burst)

Biaxial properties ('burst strength') were determined by forcing a polished stainless-steel ball (25.400 ± 0.005 mm diameter) through the sample, which was held in a clamping system containing an orifice (44.450 ± 0.025 mm diameter) per ASTM D3787-07. Samples (n = 19) were fully rehydrated via immersion in room-temperature PBS for 5 min prior to testing. Force was measured using a 2 kN load cell and extension was measured from crosshead displacement (305 mm/min).

Suture retention

Test materials were cut into 20 × 30 mm samples before a 0.35 mm nylon monofilament suture was threaded through the test sample 10 mm from the short edge with a bite-depth of 2 mm. The suture was tied off with a surgeon's loop knot to create a suture loop approximately 20 mm in diameter. Samples (n = 19) were fully rehydrated via immersion in room-temperature PBS for 5 min prior to testing. Samples were oriented with the suture on top which was looped around an aluminium hook fixture secured in the top clamp before the bottom of the sample was fixed in the bottom clamp, such that there was no pre-loaded stress/tension placed on the point at which the suture was threaded through the sample. Force was measured using a 100 N load cell and extension was measured from crosshead displacement (20 mm/min).

Molecular weight determination

The molecular weight of HA test samples was determined via size exclusion chromatography with multi-angle light scattering detection (SEC-MALS). Samples of GAGF before and after EO terminal sterilization were prepared at a nominal concentration of 0.5 mg/mL in an aqueous mobile phase buffer (30 mM phosphate buffer, 150 mM NaCl, pH 7.4). Samples of GAGF post EO exposure were taken from CMP devices. Sample solutions were filtered through 13 mm, 0.45 μm nylon syringe filters prior to SEC analysis. Injections (200 μL) were made in duplicate to a PL Aquagel-OH mixed-H columns (Agilent, Santa Clara, CA) fitted with a guard column. Samples were eluted using a mobile phase buffer at a flow rate of 0.5 mL/min, a column temperature of 40°C, a refractive index (RI) detector of 30°C and a run time of 60 min. Chromatograms were monitored using a HELEOS II multi-angle light scattering detector and Optilab T-rEX refractive index detector (Wyatt Technology, Santa Barbara, CA). Two injections per sample were performed. The specific refractive index increment (dn/dc) was measured for HA sodium salt (0.1454 ± 0.0026 mL/g) and applied to all other samples during molecular weight calculation.

Capillary viscometry

Capillary viscometry was conducted using an Ubbelohde viscometer (Size 1B) with a nominal viscometer constant of 0.05 $mm^2/s,^2$ in a water bath maintained at 30 ± 1°C. Samples of GAGF before and after EO terminal sterilization

were dissolved at a concentration of 1 mg/mL in 0.2 M aqueous NaCl solvent for 1 h prior to dilution to test concentrations (1.0–0.2 mg/mL). All samples were incubated at test temperature for at least 20 min before testing in duplicate. Flow times were analysed to determine intrinsic viscosity by extrapolating the plot of reduced viscosity versus concentration, and inherent viscosity versus concentration, to zero as follows (equations (1–3))

$$\text{Reduced Viscosity} = \eta_{\text{red}} = \frac{t - t_s/t_s}{C} \quad (1)$$

$$\text{Inherent Viscosity} = \eta_{\text{inh}} = \frac{\ln(t/t_s)}{C} \quad (2)$$

$$\text{Intrinsic Viscosity} = [\eta] = (\eta_{\text{red}})_{C\to 0} = (\eta_{\text{inh}})_{C\to 0} \quad (3)$$

Where t is the sample efflux time, t_s is the 0.2 M aqueous NaCl solvent control efflux time and C is concentration.

Moisture content

The moisture content of test samples was determined via Karl Fischer titration using an EasyPlus Moisture Analyzer (Mettler-Toledo AG, Switzerland), per AOAC 984.20 'Moisture in Oils and Fats, Karl Fischer method'. Approximately 50 mg of sample were used per repeat measurement and samples were tested in duplicate. Sample moisture content was determined on a mass basis (%w/w). The theoretical moisture content of the CMP sample could be approximated using a simple rule of mixtures equation as follows (equation (4))

$$\%MC_{\text{CMP}} = V_{\text{OFM}}\%MC_{\text{OFM}} + V_{\text{GAGF}}\%MC_{\text{GAGF}} \quad (4)$$

Where %MC is the percentage moisture content (%w/w) as derived from Karl Fischer titration, V is the volume fraction and the subscript denotes the sample and sample component. The volume fraction of CMP devices was calculated by recording the mass of a sample, then carefully separating the layers and recording the mass of the OFM layers (as one component) and the GAGF layer separately. The mass conversion to %w/w was calculated as follows (equation (5))

$$\%\text{ mass of CMP sample component } (\%w/w) = \left(\frac{\text{mass of component } (mg)}{\text{mass of CMP sample } (mg)}\right) \times 100 \quad (5)$$

Moisture retention

Test samples (50 × 50 mm) of OFM-3 and CMP devices were weighed and rehydrated via immersion for 10 min in room temperature PBS before being weighed again. Samples (n = 6) were then placed in a petri dish and incubated at 37°C. Sample mass was recorded periodically up to 80 h, and the loss of moisture was determined as a function of time as follows (equation (6))

$$\text{Moisture Mass } (\%) = 100 - \left(\frac{W_i - W_t}{W_i} \times 100\right) \quad (6)$$

Where w_i is the initial mass of the petri dish and rehydrated sample before incubation and w_t is the mass of petri dish and rehydrated sample at time t. If w_t became less than w_i at any point, the remaining percentage of moisture was taken as zero.

In vitro cell migration assay

The migration rates of human-derived immortalised HaCaT cells were assessed by the scratch assay method, according to the method of D'Agostino et al.[48] HaCaTs were seeded at 1 × 10^5 cells/well on poly-L-lysine coated 96-well plates and incubated for 48 h at 37°C and 5% CO_2 to 90% confluency in DMEM supplemented with 2% FBS. A ~1 mm scratch running through the middle of each well was created in the monolayer using a 100 µL pipette tip and cell monolayers were washed once with DMEM media (100 µL) to remove cellular debris. Test articles were cut to 2.5 × 2.5 cm samples and extracted in DMEM (4 mL) for 24 h at 37°C with gentle shaking (100 r/min). The test extracts were diluted 1:1 in DMEM with 1% FBS serum (Gibco; 10,091–148), to give a final concentration of 0.5% FBS in each extract. A media-only control (DMEM +0.5% FBS), and a positive control of DMEM +10% FBS were included in all assays. Test articles (100 µL) and controls (n = 6) were added to scratched monolayers, and the cultures imaged at 0 and 24 h using an IX51 inverted microscope (Olympus, Tokyo, Japan) fitted with a Sony NEX camera (Sony). One frame was captured per well, such that the scratch aligned vertically in the image and perpendicularly at the centre of the well. Infill of the scratch was determined by comparing the total area of the scratched cell monolayer (pixels) at 0 h and after 24 h incubation. The area of the scratch at 24 h after treatment was measured using ImageJ software and migration expressed as a percentage relative to the area at 0 h.

In vitro cell proliferation assay

Immortalised keratinocyte cells were seeded onto poly-L-lysine coated 96-well plates at 10,000 cells/well (100 µL per well) and incubated for 48 h at 37°C and 5% CO_2 to 50% confluency in DMEM supplemented with 2% FBS. Test articles were cut to 2.5 × 2.5 cm samples and extracted in DMEM (4 mL) for 24 h at 37°C with gentle shaking (100 r/min). The test extracts were diluted 1:1 in DMEM with 1% FBS serum (Gibco; 10,091–148), to give a final concentration of 0.5% FBS in each extract. A media-only

control (DMEM + 0.5% FBS), and a positive control of DMEM +10% FBS were included in all assays. Test article extracts (100 µL) and controls (n = 6) were added to wells and incubated for 48 h. Test extract/control media was removed from each well before the addition of MTT solution (100 µL of 0.5 mg/mL prepared in PBS) and plates were incubated for 2 h at 37°C. Wells were aspirated and cells lysed by addition of 150 µL of lysis buffer (1:1 DMSO: Isopropanol) and incubation for 10 min at room temperature. Lysed well contents were briefly mixed and 100 µL transferred to new 96 well plates for absorbance quantification at 570 nm using a FLUOstar Omega plate reader (BMG Labtech, Ortenberg, Germany). Cell proliferation was expressed as a percentage relative to the media only control.

Results

Retention of extracellular matrix structure and residual vascular channels

Lyophilized and terminally sterilized (EO) OFM sheets were assessed via AFM to characterize the collagen fibres architecture (Figure 2). Collagen fibres on the abluminal face of OFM were readily apparent under AFM, with distinct striations spaced regularly along each fibril, a structural characteristic of native (i.e. non-denatured or reconstituted) collagen. Dye perfusion (Figure 3(a)) enabled visualization of the residual vascular channels present in OFM, including fine microvasculature. MicroCT enabled more detailed examination of these structural features as well as the matrix architecture itself (Figure 3(b)), visualizing the ECM as an open porous matrix with heterogenous fibre diameters and pore sizes, consistent with native ECM. Residual vascular channels measuring ~0.1–1.0 mm in diameter were observed running through the luminal surface of the ECM. As shown in Figure 3(b), while some of the channels were flattened by compression, the tubular structures remained otherwise intact.

Mechanical characterization

The mechanical performance of test samples was characterized through uniaxial, biaxial (ball burst) and suture retention testing (Table 1). As expected, the maximum uniaxial load at failure increased proportionally with the number of OFM layers in the sample, with five-layered OFM-5 devices, and three-layered OFM-3 samples having an average maximum load value of 17.62 ± 7.08 N, and 12.02 ± 4.72 N, respectively. Similarly, burst strength (biaxial breaking force) and suture retention strength increased with the number of OFM layers when comparing OFM-5 devices with OFM-3 devices, whilst elastic modulus was not significantly different between the two device compositions.

The impact from the inclusion of the HA foam was also assessed via comparing the relative biophysical performance of CMP and OFM-3 devices, as both devices comprise three OFM layers. In this comparison, uniaxial strength, burst strength, suture retention strength and elastic modulus were reduced in CMP devices relative to non-HA containing OFM-3 devices (Table 1). Representative stress (%) vs strain (MPa) curves are provided in Figure 4.

Molecular weight and viscosity analysis

The molecular weight of HA in GAGF samples before and after EO terminal sterilization was determined via

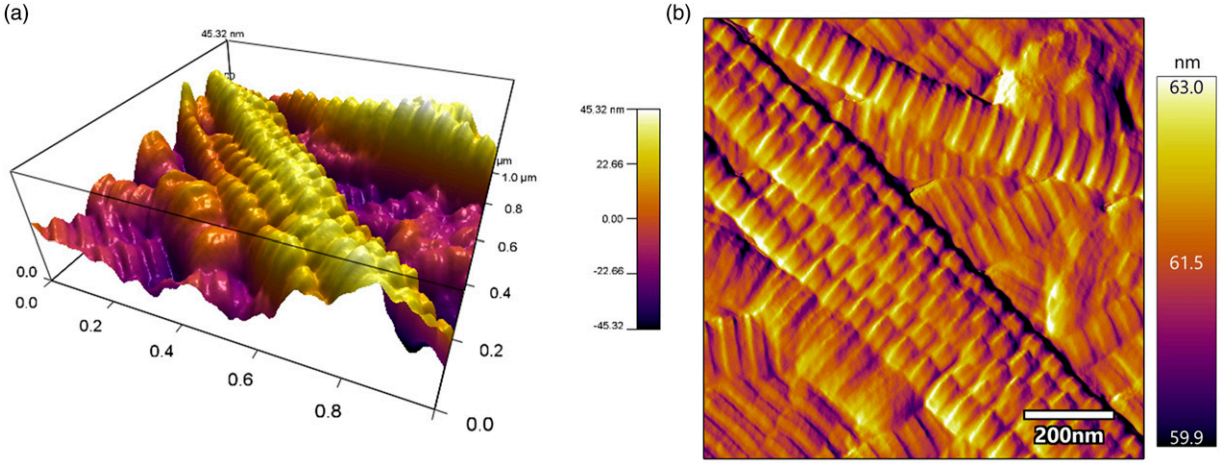

Figure 2. Visualization of OFM by atomic force microscopy. (a). 3D representation of the topography of intact collagen fibrils in the OFM material, and (b). An AFM amplitude image from the same area. OFM: Ovine forestomach matrix

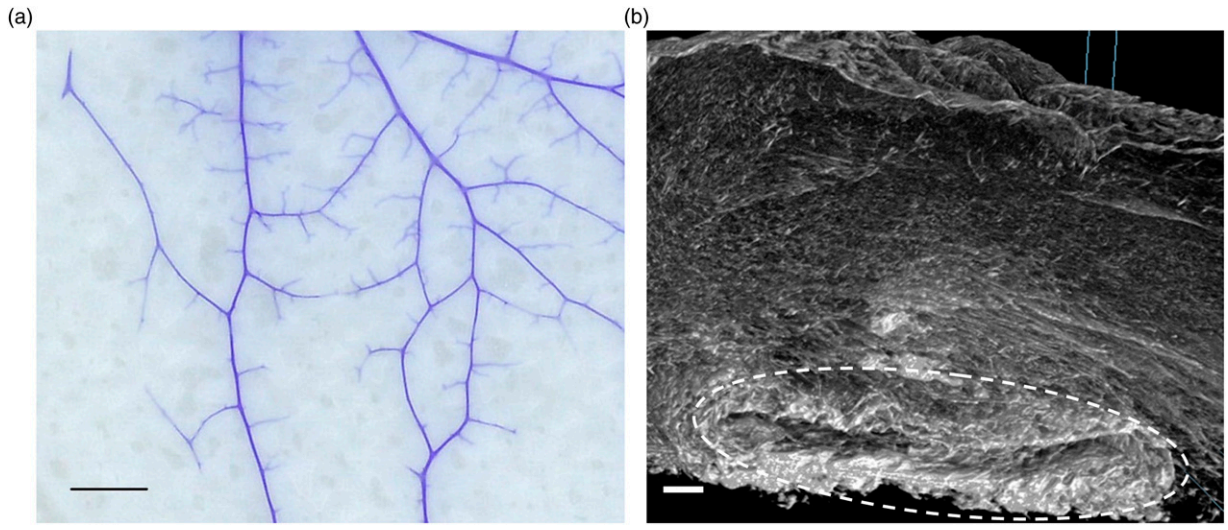

Figure 3. Representative image of residual vascular channels imaged via (a). Dye perfusion (scale bar = 10 mm) and (b). MicroCT (scale bar = 100 μm). White dotted outline indicates residual vascular channel imaged via microCT.

Table 1. Summary of biophysical properties of samples.

	OFM-3	OFM-5	CMP
Uniaxial			
Load at failure (*N*)	12.02 ± 4.72	17.62 ± 7.08	10.05 ± 3.04
Tensile strength (MPa)	1.87 ± 0.73	1.66 ± 0.62	1.21 ± 0.36*
Strain at break (%)	41.49 ± 10.04	39.69 ± 16.84	32.73 ± 10.54*
Elastic modulus (MPa)	8.05 ± 3.11	7.06 ± 2.78	6.06 ± 2.19*
Biaxial			
Breaking force (*N*)	148.54 ± 29.02	254.56 ± 42.79	111.45 ± 29.89*
Max. Displacement (mm)	29.88 ± 1.57	30.17 ± 1.16	22.44 ± 1.26*
Suture retention			
Max. Force (*N*)	10.91 ± 2.66	15.54 ± 2.37	5.28 ± 1.65*

Values represent mean and error represent the standard deviation of n = 19 replicate samples; *p < .05 via 2-sample t-test compared with OFM-3. OFM: Ovine forestomach matrix; CMP: composite samples.

SEC-MALS analysis. Post EO GAGF samples were taken from finished CMP devices. Weight average molecular weight (Mw), number average molecular weight (Mn) and polydispersity (Mw/Mn) are presented in Table 2. Exposure of the GAGF to EO sterilization resulted in an approximately 40% reduction in the weight average molecular weight of the HA.

Observed changes in the HA molecular weight were confirmed via capillary viscometry analysis of HA before and after EO exposure (Figure 5). The intrinsic viscosity (η) of HA in terminally sterile CMP samples was determined as 7.71 ± 0.07 dL/g, while the intrinsic viscosity of HA prior to EO exposure was 12.06 ± 0.33 dL/g (Table 2).

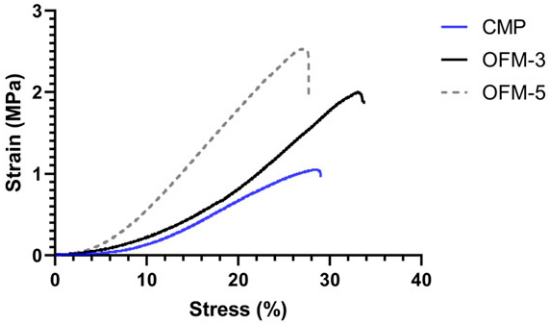

Figure 4. Representative stress (%) vs strain (MPa) curves for OFM-3, OFM-5 and CMP devices.

Moisture content and retention

The moisture content (%MC) of OFM, GAGF and CMP samples was determined through Karl-Fischer titration, demonstrating individual device components (OFM and GAGF) differ in %MC with the CMP sample (Table 3). The higher moisture content of GAGF and CMP devices was attributed to the highly hygroscopic nature of HA. A 2-sample t-test analysis of OFM and GAGF components compared with the CMP sample produced p-values of < .001. However, by applying the rule of mixtures (typically used for modulus determination in fibre reinforced composite materials), it is evident that the moisture content of

Table 2. Molecular weight and polydispersity of hyaluronic acid in ethylene oxide terminally sterilized GAGF (taken from a CMP sample) ('Post-EO'), and GAGF prior to ethylene oxide terminal sterilization ('Pre-EO').

GAGF Condition	Weight average molecular weight Mw (kDa)	Number average molecular weight Mn (kDa)	Polydispersity Mw/ Mn	Intrinsic viscosity (η) (mL/g)
Pre-EO	1070 ± 7	788 ± 1	1.4 ± 0.1	12.06 ± 0.33
Post-EO	656 ± 1	411 ± 2	1.6 ± 0.1	7.71 ± 0.07

Values represent average and standard deviations from duplicate samples; EO: ethylene oxide; Mn: average molecular weight; Mw: average polydispersity

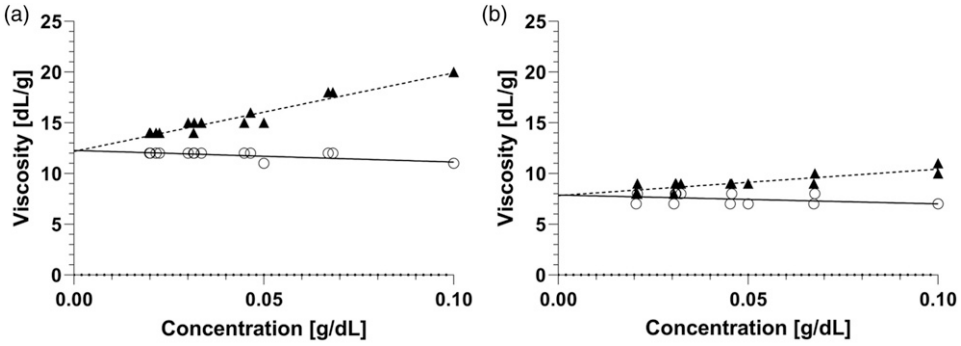

Figure 5. Viscosity determination of HA in GAGF samples (taken from CMP devices) before (a) and after (b) ethylene oxide terminal sterilization. Reduced viscosity (solid markers) and inherent viscosity (open markers). GAGF: glycosaminoglycan foam; CMP: composite samples.

Table 3. Moisture content of components (OFM-3 and GAGF) CMP.

	OFM	GAGF	CMP
Moisture content (%w/w)	15.92 ± 1.46	18.79 ± 1.28	16.81 ± 0.96

Values represent average and errors represent the standard deviation of; OFM, n = 60; GAGF, n = 19; CMP, n = 19 replicate samples.
OFM: Ovine forestomach matrix; GAGF: glycosaminoglycan foam; CMP: composite samples.

the CMP sample is a product of both components (OFM and GAGF). The average volume fraction of OFM and GAGF components in a CMP sample were 0.68 and 0.32, respectively. Using the derived %MC data for the OFM and GAGF components the theoretical CMP sample %MC according to the rule of mixtures equalled 16.84%, equivalent to the experimentally derived %MC value for CMP samples (16.81%).

The mass of rehydrated OFM-3 and CMP samples was measured over time following incubation at 37°C and the percentage moisture remaining in the sample as a function of time determined (Figure 6). Moisture loss was linear over the time course, indicated by linear regression R^2 values of 0.84 (OFM-3) and 0.97 (CMP). OFM-3 samples showed complete moisture loss by approximately 40 h, while CMP samples containing the GAGF layer retained moisture to approximately 80 h (Figure 6).

Keratinocyte migration and proliferation

Terminally sterilized samples of OFM-3, GAGF and CMP devices were extracted in cell culture media to assess their impact on keratinocyte migration and proliferation *in vitro*. Keratinocyte monolayers treated with CMP or GAGF extracts demonstrated a statistically significant ($p < .0001$) increase in scratch closure (69 ± 13% and 85 ± 17%, respectively) compared to media-only controls and OFM-3 treated monolayers (36 ± 11%) (Figure 7).

Keratinocytes treated with OFM, CMP or GAGF extracts demonstrated statistically significant ($p = .0001$ and $p < .0001$) increases in keratinocyte proliferation (139 ± 56%, 158 ± 53% and 183 ± 57%, respectively) compared to media-only controls. The addition of HA to the OFM-3 sample gave a statistically significant increase in proliferation ($p < .01$), as expected due to the known proliferative bioactivity of HA (Figure 8).

Discussion

A key philosophy driving the design of modern dECM biomaterials is maximizing retention of native tissue ECM structure, biology and hence function. Previous studies demonstrate that the structure of OFM is consistent with that of native tissue ECM, as determined via differential scanning calorimetry (DSC),[6] scanning electron microscopy (SEM),[5,6] histology,[5] Sirius Red staining[6] and small-angle

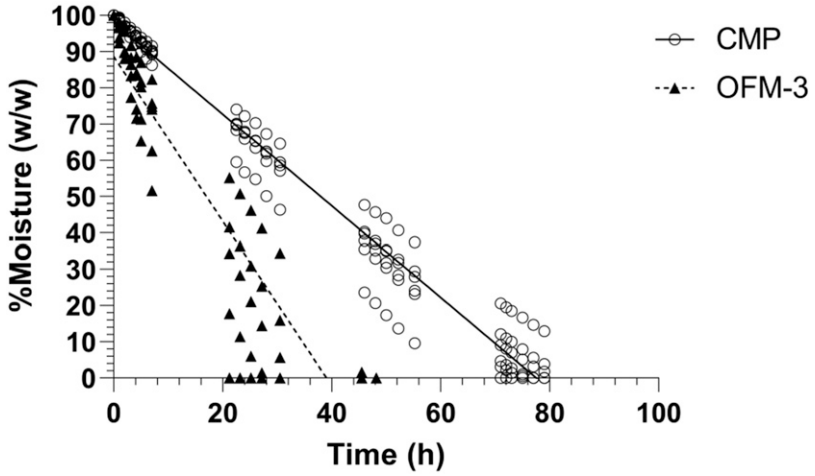

Figure 6. Moisture retention of OFM-3 and CMP samples as a function of time at 37°C. Six replicates per sample, per time point. Lines represent linear regression (CMP R2 = 0.97; OFM-3 R2 = 0.84). OFM: Ovine forestomach matrix-3; CMP: composite samples. OFM: Ovine forestomach matrix-3; CMP: composite samples.

X-ray scattering (SAXS).[6,10] OFM has also previously been shown to have a total GAG concentration of 0.74 ± 0.01 mg/g with a diffuse distribution throughout the ECM, thus highlighting the preservation of the natural ECM .[5] The current analysis utilized AFM to characterize the collagen fibre striations and periodicity, and microCT to visualize the matrix architecture including residual vascular channels. The AFM analysis further verified the native collagen fibre architecture of OFM, consistent with the results of previous DSC and SAXS analyses.[6,10] Via microCT, the OFM bioscaffold appeared as a complex matrix of irregularly sized fibrous proteins forming a network of open heterogeneous pores, characteristic of tissue ECM.[49] Both microCT and dye perfusion enabled visualization of the residual vascular channels running through OFM. The ovine forestomach is a uniquely vascular tissue that has evolved to be the primary means of nutrient absorption for ruminants. As such, the forestomach tissue is highly vascular with a high density of capillaries and associated microvascular networks relative to other tissues.[50] Additionally, the capillaries of ovine forestomach are fenestrated with pores to facilitate the absorptive functions of the rumen.[27] The process of OFM decellularization is designed to selectively remove ovine cells, including endothelial cells, while retaining the structure and composition of the ECM. Recellularization studies demonstrate that dECM scaffolds repopulate in an organized fashion, with the dECM providing localized cues to guide repopulation.[51] For example, endothelial cells have been shown to preferentially line remnant vessels in decellularized heart tissue.[52] With the vascular network and associated endothelial basement membrane of OFM preserved,[5] it is hypothesized that during the repair process the residual vascular channels serve as a template for the patients' endothelial cells to enable rapid repopulation and revascularization of the OFM grafts.[53–55] The process of endothelial repopulation is aided by endothelial basement components including collagen IV, laminin, as well as specialist basement membrane components, for example perlecan.[8] Perlecan is a basement membrane specific heparan sulphate proteoglycan which binds multiple growth factors and other ECM proteins, with multiple functional roles including angiogenesis.[56] The term 'angioconduction' has previously been used to describe the phenomenon of vascular templating seen by bone grafts,[57,58] and draws parallels to 'osteoconduction', whereby the physical architecture of bone scaffolds direct osteogenesis.[59] Angioconduction describes a similar process where the physical structure of a material directs and promotes angiogenesis.[57,58,60,61] Angioconduction may be demonstrated using the chicken chorioallantoic membrane (CAM)[61] assay. Our previous work using this assay showed the angioconductive properties of OFM resulting from the residual vascular channels (Figure 3). This phenomenon has been shown to lead to greater capillary density and vascularity in vivo .[7]

The interlock fabrication process described herein represents a novel alternative to the approaches traditionally used to fabricate multi-layered dECM devices. The current approach was envisaged to create dECM grafts for non-load bearing applications, for example, dermal reconstruction, periosteal wraps and hemostats. This multi-layered fabrication approach offers some clear advantages to existing methods, namely, the absence any foreign materials (e.g. chemical crosslinking agents or adhesives); creation of open pores, interstices and channels through the device material to support rapid cell infiltration; and flexibility in thickness and composition allowing a diversity of device designs tailored to specific clinical applications. Certain dECM

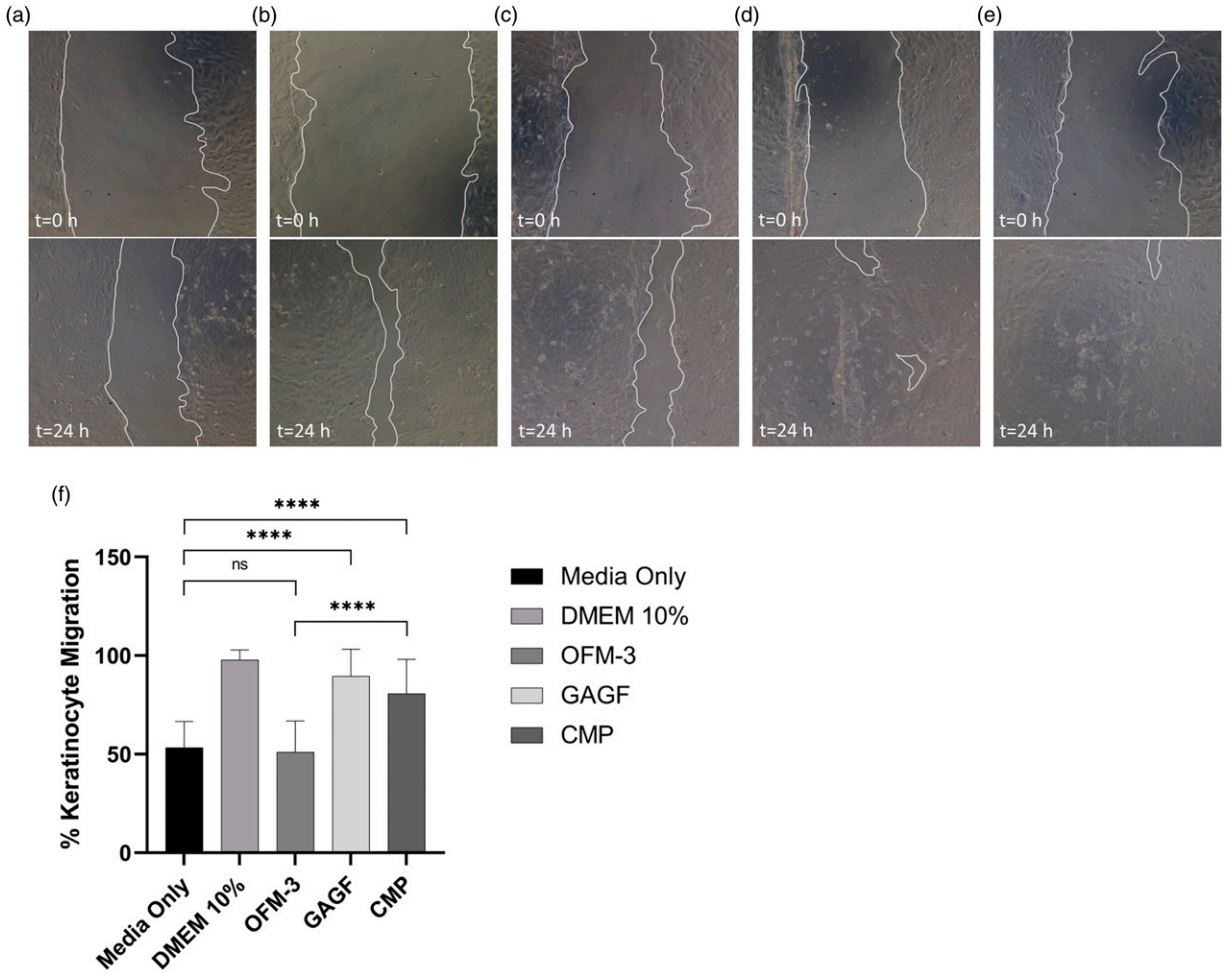

Figure 7. In vitro human keratinocyte migration. Representative images of scratched mono-layers at t = 0 h and t = 24 h for the test samples, media only (a), DMEM +10% serum (b), OFM-3 (c), HA (d), and CMP (e), (f) Quantification of average percent epithelial migration. Error bars represent standard deviation from triplicate independent experiments with n = 6 sample replicates per experiment. ****, $p < .0001$; ns = not significant. DMEM: Dulbeccós modified Eaglés Medium; OFM: Ovine forestomach matrix-3; CMP: composite samples.

grafts suffer from poor cell infiltration kinetics, typically due to the density of the matrix that may hinder cell migration and vascularization. This is particularly apparent in thicker and less permeable dECM devices where the reduced rates of recellularization leave acellular zones within the implanted grafts.[11] The kinetics of cell infiltration can be increased via engineered perforations to the dECM, enabling cells to more rapidly absorb into, and migrate through the graft, a feature that has been shown clinically in soft tissue and abdominal wall reconstructions.[11,19,62] The interlocking process introduced open pores that transect the OFM layers increasing the effective surface area of the device. Additionally, the interlocking process and the resultant approximation of opposing OFM layers form channels or openings between layers that further enable the lateral spread of cells.

Samples prepared by the interlock process had a reduced strength (uniaxial ~10–20 *N*; burst strength ~100–300 *N*) compared to OFM-based devices embroidered with PGA suture material (uniaxial~10–60 *N*; burst strength~200–1000 *N*).[10] This is attributed to the high tensile strength and modulus of braided PGA suture which the load is imparted onto during testing of embroidered devices. Importantly though, the suture retention strengths of interlock samples (OFM-5; 15.54 ± 2.37 *N*) compared well to embroidered devices (6-ply laminate, 4–0 suture sewn; 13.33 ± 1.22 *N*),[10] and are therefore expected to resist suture pull-out once fastened to the soft tissue defect. An unexpected advantage of the interlock process and the resultant devices was the relative decrease in elastic modulus of samples. Interlocked samples had a modulus of elasticity of <10 MPa, while OFM devices embroidered with PGA suture material,

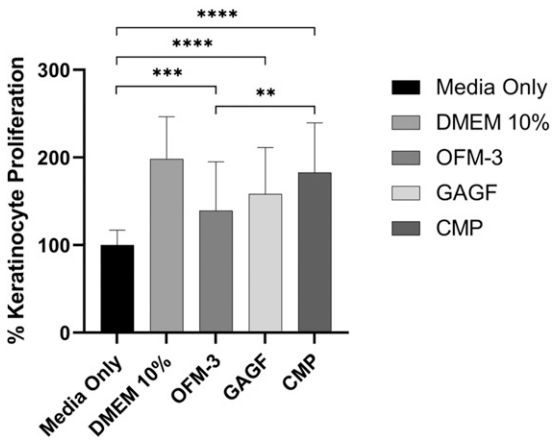

Figure 8. In vitro human keratinocyte proliferation. Quantification of average percent change in proliferation, relative to the media-only control. Error bars represent standard deviation from triplicate independent experiments with $n = 6$ sample replicates per experiment. ***, $p = .0001$; ****, $p < .0001$ relative to the media only control; **, $p < .01$ CMP sample versus OFM-3 sample. OFM: Ovine forestomach matrix-3; CMP: composite samples.

laminated using adhesives or chemical crosslinks have a reported modulus of elasticity of >30 MPa.[10] This increase in elasticity (reduction in modulus) may be attributed to the relatively open structure of samples prepared by the interlock method, whereby opposing layers are not bonded continuously across all surfaces, but rather are held in place via the tabs at 3.5 mm intervals. This enables sheets to move relatively independently of one another when under load.

The interlocking process enables the incorporation of additional layers of materials to provide additional functionality that can be used to create composite dECM-based devices for specific clinical applications. In the example provided, HA, as a single layer of foam was included to create a composite device. HA was chosen for this exemplification based on its established biology in relation to dermal regeneration. A naturally occurring biomolecule present in the ECM, and OFM,[5] HA has various roles in soft tissue repair processes including angiogenesis, cell migration and moisture retention.[63–66] The angiogenic properties of smaller MW HA fragments (<600 kDa) are well described in the literature,[67,68] and affect accelerated wound healing.[69] Hodgkinson and Bayat described the addition of HA to a synthetic graft to stimulate keratinocyte migration and increase wound closure rates.[70] HA is extremely hydrophilic and can sequester ~1000 times its weight in water to form a hydrogel material, providing that the entanglement density is sufficient for gelation.[71] Given its prominent role in soft tissue repair mechanisms HA has been included in a large number of cutaneous wound repair products.[72]

In vivo, high molecular weight (HMW) HA (>1000 kDa) is present in tissue during homoeostasis and turns over at a high rate via degradation to smaller fragments including medium molecular weight (MMW) (250–1000 kDa), low molecular weight (LMW) (10–250 kDa) and oligo-HA (0.01–10 kDa). At different stages of wound healing, HA is present in a polydisperse state of different molecular masses, the ratios of this pool of HA fragments will differ giving distinct but overlapping cellular responses. Generally, HMW HA directs the control of inflammation and maintenance of tissue integrity while oligo-HAs induce inflammatory responses, angiogenesis, elastin synthesis and keratinocyte proliferation and migration.[69,73] LMW and MMW have biological roles that overlap the two ends of this spectrum and include increases in ECM deposition and cell differentiation.[74] This work indicates that EO sterilization lowers the average MW of the HA in the foam; however, the dispersity indicates that the foam contains both high and low MW fragments, both of which facilitate wound healing processes in an overlapping and complementary manner. Importantly, by retaining high MW HA-sterilized composite devices *in situ* can act as a reservoir, providing a cache of HA for metabolism into functional products for tissue repair processes as directed by cellular and enzymatic activities.

The uniaxial strength (Load at Failure) of the HA-containing samples ('CMP') were equivalent to OFM-3 (Table 1), while the tensile strength, strain at break and elastic modulus were reduced due to the increase in sample cross-sectional area as a result of the HA foam layer. Additionally, the biaxial break force (*N*) and suture retention force (*N*) were reduced following the addition of the HA layer to OFM-3 samples (Table 1). CMP devices demonstrated clinically relevant properties in resisting suture pull out, with all CMP device results above the recommended suture retention strength of 2 *N*.[75]

Due to HA's high affinity for water, it was hypothesized that composite devices would retain moisture for greater time periods compared to interlocked samples prepared from OFM material alone. Moisture retention of dECM grafts is an important design aspect for soft tissue reconstruction as the ability for a graft to maintain a moist wound environment promotes cell migration, reduces scarring and fibrosis, and improves angiogenesis.[76] *In vitro* testing herein was intended to reflect a 'worst case' scenario, with no moisture added to the test sample after initial hydration. As expected, the addition of the HA layer to the CMP samples improved the device moisture retention properties, approximately doubling the time to complete moisture loss of the device (Figure 6).

In vitro testing demonstrated that inclusion of HA into CMP devices induced changes in the biological response to the device, as measured through cellular migration and proliferation of keratinocytes. Cutaneous wound healing involves haemostasis, inflammation, granulation, reepithelialisation, and contraction/tissue remodelling.[77] In dermal wound healing, reepithelialisation involves the migration and proliferation of keratinocytes to cover and replace the epithelial layer

above the remodelling tissue of the wound. In addition to forming the keratin layer of dermal tissue, keratinocytes have several other critical roles in wound healing.[78] In human skin, keratinocytes are formed in the stratum basale and migrate vertically until reaching the superficial stratum corneum to be shed. It is hypothesized, that multi-layer dECM fabricated with sufficient channels for cell migration would allow for better cell migration both laterally and vertically. Synthetic, crossed-linked and vacuum-baked methods inherently are not conducive for the migration of cells due to the nature of the layering process. Keratinocytes recruit, stimulate, and coordinate the actions of multiple cell types involved in healing and recapitulate the epidermal barrier layer of the skin.[77] Keratinocytes release pre-stored interleukin 1 (IL-1) in response to the disruption of the epidermal barrier, which acts as both an autocrine and paracrine signal that mobilizes surrounding cells to aid in healing.[79] Keratinocytes also secrete angiogenic growth factors, such as vascular endothelial growth factor (VEGF) and platelet-derived growth factor (PDGF),[80] which induce endothelial cell migration and angiogenesis in the wound bed,[81] and, in the case of PDGF, promote fibroblast proliferation and production of extracellular matrix.[79] Due to these functions, proteins and glycosaminoglycans which stimulate the migration and proliferation of keratinocytes are likely to improve wound healing outcomes in patients. Further in vivo studies are ongoing to assess the impact of CMP devices on wound closure rates and validate the observed in vitro impact on keratinocyte migration and proliferation. Additionally, further testing is recommended to evaluate if this novel method of creating multi-layered dECM would be applicable and effective using other xenograft source material as well as human-derived allograft materials. Only OFM-based devices were evaluated in this study and further study would need to be conducted to determine if the purposed method of creating multi-layer dECM device would be effective when using various source materials for dECM.

Conclusions

This study demonstrates that multi-layered dECM devices with clinically useful compositional and biomechanical properties may be fabricated without the inclusion of additional bonding materials or ECM modifying treatments that compromise regenerative potential. Furthermore, this work shows that incorporation of supplementary material layers into interlocked OFM devices can be employed to enhance the device functionality. Such devices with unimpaired regenerative potential of native ECM and capacity for finely tuned functional properties are of promising utility in tissue repair applications.

Declaration of conflicting interests

The author(s) declared the following potential conflicts of interest with respect to the research, authorship, and/or publication of this article: MJS, SGD, RWFV, MJJ, AN, AJ, IM, RGS, CHM, and BCHM are shareholders of Aroa Biosurgery Limited (New Zealand).

Funding

The author(s) disclosed receipt of the following financial support for the research, authorship, and/or publication of this article: This work was supported by Aroa Biosurgery and Callaghan Innovation (Growth Grant MSMA1402).

ORCID iD

Barnaby C H May https://orcid.org/0000-0001-9855-018X

References

1. Badylak SF. The extracellular matrix as a biologic scaffold material. *Biomaterials* 2007; 28: 3587–3593.
2. Badylak S, Freytes D and Gilbert T. Extracellular matrix as a biological scaffold material: structure and function. *Acta Biomater* 2009; 5: 1–13.
3. Franklin ME Jr, Treviño JM, Portillo G, et al. The use of porcine small intestinal submucosa as a prosthetic material for laparoscopic hernia repair in infected and potentially contaminated fields: long-term follow-up. *Surg Endosc* 2008; 22: 1941–1946.
4. Wainwright DJ. Use of an acellular allograft dermal matrix (AlloDerm) in the management of full-thickness burns. *Burns* 1995; 21: 243–248.
5. Lun S, Irvine SM, Johnson KD, et al. A functional extracellular matrix biomaterial derived from ovine forestomach. *Biomaterials* 2010; 31: 4517–4529.
6. Sizeland KH, Wells HC, Kelly SJR, et al. Collagen fibril response to strain in scaffolds from ovine forestomach for tissue engineering. *ACS Biomater Sci Eng* 2017; 3: 2550–2558.
7. Irvine SM, Cayzer J, Todd EM, et al. Quantification of in vitro and in vivo angiogenesis stimulated by ovine forestomach matrix biomaterial. *Biomaterials* 2011; 32: 6351–6361.
8. Dempsey SG, Miller CH, Hill RC, et al. Functional insights from the proteomic inventory of ovine forestomach matrix. *J Proteome Res* 2019; 18: 1657–1668.
9. Dempsey SG, Miller CH, Schueler J, et al. A novel chemotactic factor derived from the extracellular matrix protein decorin recruits mesenchymal stromal cells in vitro and in vivo. *PLoS One* 2020; 15: e0235784.
10. Floden EW, Malak SFF, Basil-Jones MM, et al. Biophysical characterization of ovine forestomach extracellular matrix biomaterials. *J Biomed Mater Res B: Appl Biomater* 2010; 96B: 67–75.

11. Overbeck N, Nagvajara GM, Ferzoco S, et al. In-vivo evaluation of a reinforced ovine biologic: a comparative study to available hernia mesh repair materials. *Hernia* 2020; 24: 1293–1306.
12. Karnik T, Dempsey SG, Jerram MJ, et al. Ionic silver functionalized ovine forestomach matrix - a non-cytotoxic antimicrobial biomaterial for tissue regeneration applications. *Biomater Res* 2019; 23: 6.
13. Raizman R, Hill R and Woo K. Prospective multicenter evaluation of an advanced extracellular matrix for wound management. *Adv Skin Wound Care* 2020; 33: 437–444.
14. Liden BA and May BCH. Clinical outcomes following the use of ovine forestomach matrix (endoform dermal template) to treat chronic wounds. *Adv Skin Wound Care* 2013; 26: 164–167.
15. Bohn GA and Gass K. Leg ulcer treatment outcomes with new ovine collagen extracellular matrix dressing. *Adv Skin Wound Care* 2014; 27: 448–454.
16. Ferreras DT, Craig S and Malcomb R. Use of an ovine collagen dressing with intact extracellular matrix to improve wound closure times and reduce expenditures in a US military veteran hospital outpatient wound center. *Surg Technol Int* 2017; 30: 61–69.
17. Lullove EJ. Use of ovine-based collagen extracellular matrix and gentian violet/methylene blue antibacterial foam dressings to help improve clinical outcomes in lower extremity wounds: a retrospective cohort study. *Wounds : a Compend Clin Res Pract* 2017; 29: 107–114.
18. Chaffin AE and Buckley M-C. Extracellular matrix graft for the surgical management of Hurley stage III hidradenitis suppurativa: a pilot case series. *J Wound Care* 2020; 29: 624–630.
19. Bohn GA and Chaffin AE. Extracellular matrix graft for reconstruction over exposed structures: a pilot case series. *J Wound Care* 2020; 29: 742–749.
20. Simcock J and May BC. Ovine forestomach matrix as a substrate for single-stage split-thickness graft reconstruction. *Eplasty* 2013; 13: e58.
21. Desvigne MN, Bauer K, Holifield K, et al. Case report: surgical closure of chronic soft tissue defects using extracellular matrix graft augmented tissue flaps. *Front Surg* 2020; 7: 559450.
22. Ferzoco SJ. Early experience outcome of a reinforced Bioscaffold in inguinal hernia repair: a case series. *Int J Surg Open* 2018; 12: 9–11.
23. Parker MJ, Kim RC, Barrio M, et al A novel biosynthetic scaffold mesh reinforcement affords the lowest hernia recurrence in the highest-risk patients. *Surg Endosc* 2020; 35: 5173–5178.
24. Malcarney HL, Bonar F and Murrell GAC. Early inflammatory reaction after rotator cuff repair with a porcine small intestine submucosal implant. *The Am J Sports Med* 2005; 33: 907–911.
25. Zheng MH, Chen J, Kirilak Y, et al. Porcine small intestine submucosa (SIS) is not an acellular collagenous matrix and contains porcine DNA: possible implications in human implantation. *J Biomed Mater Res Part B: Appl Biomater* 2005; 73B: 61–67.
26. Easterbrook C and Maddern G. Porcine and bovine surgical products. *Arch Surg* 2008; 143: 366–370.
27. Karmona Kh and Kovachev G. Ultrastructure of the subepithelial capillaries and venules in the forestomach of sheep. *Veterinarno-meditsinski nauki* 1986; 23: 42–51.
28. Freytes DO, Badylak SF, Webster TJ, et al. Biaxial strength of multilaminated extracellular matrix scaffolds. *Biomaterials* 2004; 25: 2353–2361.
29. Badylak SF and Gilbert TW. Immune response to biologic scaffold materials. *Semin Immunol* 2008; 20: 109–116.
30. Rowley AT, Nagalla RR, Wang SW, et al. Extracellular matrix-based strategies for immunomodulatory biomaterials engineering. *Adv Healthc Mater* 2019; 8: e1801578.
31. Zerris VA, James KS, Roberts JB, et al. Repair of the dura mater with processed collagen devices. *J Biomed Mater Res Part B: Appl Biomater* 2007; 83B: 580–588.
32. Vardar E, Larsson HM, Engelhardt EM, et al. IGF-1-containing multi-layered collagen-fibrin hybrid scaffolds for bladder tissue engineering. *Acta Biomater* 2016; 41: 75–85.
33. Crapo PM, Gilbert TW and Badylak SF. An overview of tissue and whole organ decellularization processes. *Biomaterials* 2011; 32: 3233–3243.
34. Gilbert TW, Sellaro TL and Badylak SF. Decellularization of tissues and organs. *Biomaterials* 2006; 27: 3675–3683.
35. Naimark WA, Pereira CA, Tsang K, et al. HMDC crosslinking of bovine pericardial tissue: a potential role of the solvent environment in the design of bioprosthetic materials. *J Mater Sci Mater Med* 1995; 6: 235–241.
36. Petter-Puchner AH, Fortelny RH, Walder N, et al. Adverse effects associated with the use of porcine cross-linked collagen implants in an experimental model of incisional hernia repair. *J Surg Res* 2008; 145: 105–110.
37. Krzyszczyk P, Schloss R, Palmer A, et al. The role of macrophages in acute and chronic wound healing and interventions to promote pro-wound healing phenotypes. *Front Physiol* 2018; 9: 419.
38. Valentin JE, Badylak JS, McCabe GP, et al. Extracellular matrix bioscaffolds for orthopaedic applications. *The J Bone Jt Surg* 2006; 88: 2673–2686.
39. Valentin JE, Stewart-Akers AM, Gilbert TW, et al. Macrophage participation in the degradation and remodeling of extracellular matrix scaffolds. *Tissue Eng A* 2009; 15: 1687–1694.
40. Delgado LM, Bayon Y, Pandit A, et al. To cross-link or not to cross-link? Cross-linking associated foreign body response of collagen-based devices. *Tissue Eng B: Rev* 2015; 21: 298–313.
41. Al-Maawi S, Vorakulpipat C, Orlowska A, et al. In vivo implantation of a bovine-derived collagen membrane leads to changes in the physiological cellular pattern of wound healing

by the induction of multinucleated giant cells: an adverse reaction?. *Front Bioeng Biotechnol* 2018; 6: 104.
42. Zhang L, Niu X, Sun L, et al. Immune response of bovine sourced cross-linked collagen sponge for hemostasis. *J Biomater Appl* 2018; 32: 920–931.
43. Collins MN and Birkinshaw C. Hyaluronic acid based scaffolds for tissue engineering-a review. *Carbohydr Polym* 2013; 92: 1262–1279.
44. Patrulea V, Laurent-Applegate LA, Ostafe V, et al. Polyelectrolyte nanocomplexes based on chitosan derivatives for wound healing application. *Eur J Pharmaceutics Biopharmaceutics* 2019; 140: 100–108.
45. Li H, Xue Y, Jia B, et al. The preparation of hyaluronic acid grafted pullulan polymers and their use in the formation of novel biocompatible wound healing film. *Carbohydr Polym* 2018; 188: 92–100.
46. Tavianatou AG, Caon I, Franchi M, et al. Hyaluronan: molecular size-dependent signaling and biological functions in inflammation and cancer. *The FEBS J* 2019; 286: 2883–2908.
47. Boukamp P, Petrussevska RT, Breitkreutz D, et al. Normal keratinization in a spontaneously immortalized aneuploid human keratinocyte cell line. *The J Cel Biol* 1988; 106: 761–771.
48. D'Agostino A, Stellavato A, Busico T, et al. In vitro analysis of the effects on wound healing of high- and low-molecular weight chains of hyaluronan and their hybrid H-HA/L-HA complexes. *BMC Cel Biol* 2015; 16: 19.
49. Walton LA, Bradley RS, Withers PJ, et al. Morphological characterisation of unstained and intact tissue microarchitecture by x-ray computed micro- and nano-tomography. *Scientific Rep* 2015; 5: 10074.
50. Rémond D, Meschy F and Boivin R. Metabolites, water and mineral exchanges across the rumen wall: Mechanisms and regulation. *Ann de Zootechnie* 1996; 45: 97–119.
51. Kim JJ, Hou L and Huang NF. Vascularization of three-dimensional engineered tissues for regenerative medicine applications. *Acta Biomater* 2016; 41: 17–26.
52. Sánchez PL, Fernández-Santos ME, Costanza S, et al. Acellular human heart matrix: a critical step toward whole heart grafts. *Biomaterials* 2015; 61: 279–289.
53. Greaves NS, Morris J, Benatar B, et al. Acute cutaneous wounds treated with human decellularised dermis show enhanced angiogenesis during healing. *PLoS One* 2015; 10: e0113209.
54. Brown BN, Chung WL, Almarza AJ, et al. Inductive, scaffold-based, regenerative medicine approach to reconstruction of the temporomandibular joint disk. *J Oral Maxillofacial Surg* 2012; 70: 2656–2668.
55. Brown BN and Badylak SF. Extracellular matrix as an inductive scaffold for functional tissue reconstruction. *Translational Res* 2014; 163: 268–285.
56. Melrose J, Hayes AJ, Whitelock JM, et al. Perlecan, the "jack of all trades" proteoglycan of cartilaginous weight-bearing connective tissues. *Bioessays* 2008; 30: 457–469.
57. Rather HA, Jhala D and Vasita R. Dual functional approaches for osteogenesis coupled angiogenesis in bone tissue engineering. *Mater Sci Eng C* 2019; 103: 109761.
58. Lu Y, Lu X, Li M, et al. Minimally invasive treatment for osteonecrosis of the femoral head with angioconductive bioceramic rod. *Int Orthopaedics* 2018; 42: 1567–1573.
59. Weber FE. Reconsidering osteoconduction in the era of additive manufacturing. *Tissue Eng Part B: Rev* 2019; 25: 375–386.
60. Appleford MR, Oh S, Oh N, et al. In vivostudy on hydroxyapatite scaffolds with trabecular architecture for bone repair. *J Biomed Mater Res A* 2009; 89A: 1019–1027.
61. Magnaudeix A, Usseglio J, Lasgorceix M, et al. Quantitative analysis of vascular colonisation and angio-conduction in porous silicon-substituted hydroxyapatite with various pore shapes in a chick chorioallantoic membrane (CAM) model. *Acta Biomater* 2016; 38: 179–189.
62. Sawyer M, Ferzoco S and DeNoto G 3rd. A polymer-biologic hybrid hernia construct: review of data and early experiences. *Polymers* 2021; 13: 1928.
63. Stern R, Asari AA and Sugahara KN. Hyaluronan fragments: an information-rich system. *Eur J Cel Biol* 2006; 85: 699–715.
64. Frenkel JS. The role of hyaluronan in wound healing. *Int Wound J* 2014; 11: 159–163.
65. Fouda MMG, Abdel-Mohsen AM, Ebaid H, et al. Wound healing of different molecular weight of hyaluronan; in-vivo study. *Int J Biol Macromolecules* 2016; 89: 582–591.
66. Galeano M, Polito F, Bitto A, et al. Systemic administration of high-molecular weight hyaluronan stimulates wound healing in genetically diabetic mice. *Biochim Biophys Acta (Bba) - Mol Basis Dis* 2011; 1812: 752–759.
67. Mondalek FG, Ashley RA, Roth CC, et al. Enhanced angiogenesis of modified porcine small intestinal submucosa with hyaluronic acid-poly(lactide-co-glycolide) nanoparticles: from fabrication to preclinical validation. *J Biomed Mater Res A* 2010; 94: 712–719.
68. West D, Hampson I, Arnold F, et al. Angiogenesis induced by degradation products of hyaluronic acid. *Science* 1985; 228: 1324–1326.
69. Gao F, Liu Y, He Y, et al. Hyaluronan oligosaccharides promote excisional wound healing through enhanced angiogenesis. *Matrix Biol* 2010; 29: 107–116.
70. Hodgkinson T and Bayat A. In vitro and ex vivo analysis of hyaluronan supplementation of Integra® dermal template on human dermal fibroblasts and keratinocytes. *J Appl Biomater Funct Mater* 2016; 14: 9–18.
71. Schanté CE, Zuber G, Herlin C, et al. Chemical modifications of hyaluronic acid for the synthesis of derivatives for a broad range of biomedical applications. *Carbohydr Polym* 2011; 85: 469–489.
72. Allison DD and Grande-Allen KJ. Review. hyaluronan: a powerful tissue engineering tool. *Tissue Eng* 2006; 12: 2131–2140.

73. Gao Y, Sun Y, Yang H, et al. A low molecular weight hyaluronic acid derivative accelerates excisional wound healing by modulating pro-inflammation, promoting epithelialization and neovascularization, and remodeling collagen. *Int J Mol Sci* 2019; 20.
74. Monslow J, Govindaraju P and Pure E. Hyaluronan - a functional and structural sweet spot in the tissue microenvironment. *Front Immunol* 2015; 6: 231.
75. Billiar K, Murray J, Laude D, et al. Effects of carbodiimide crosslinking conditions on the physical properties of laminated intestinal submucosa. *J Biomed Mater Res* 2001; 56: 101–108.
76. Roehrs H, Stocco JGD, Pott F, et al Dressings and topical agents containing hyaluronic acid for chronic wound healing. *Cochrane Database Syst Rev* 2016; 5: CD012215. DOI: 10.1002/14651858.CD012215.
77. Wojtowicz AM, Oliveira S, Carlson MW, et al. The importance of both fibroblasts and keratinocytes in a bilayered living cellular construct used in wound healing. *Wound Repair Regen* 2014; 22: 246–255.
78. Pastar I, Stojadinovic O and Tomic-Canic M. Role of keratinocytes in healing of chronic wounds. *Surg Technol Int* 2008; 17: 105–112.
79. Barrientos S, Stojadinovic O, Golinko MS, et al. Perspective article: growth factors and cytokines in wound healing. *Wound Repair Regen* 2008; 16: 585–601.
80. Werner S, Krieg T and Smola H. Keratinocyte-fibroblast interactions in wound healing. *J Invest Dermatol* 2007; 127: 998–1008.
81. Bao P, Kodra A, Tomic-Canic M, et al. The role of vascular endothelial growth factor in wound healing. *J Surg Res* 2009; 153: 347–358.